

1 **Supplementary Materials**

2
3 **Iron-loaded carbonized spent bleaching earth (Fe-SBE/C)**
4 **composite used for arsenic removal from water**

5
6 **Siswanti Puji¹, Juntao Guo¹, Yihui Zhang¹, Kexin Song¹, Feng Wu^{1,*}, Jing Li^{2,*}**

7 ¹Hubei Key Lab of Biomass Resource Chemistry and Environmental Biotechnology,
8 School of Resources and Environmental Science, Wuhan University, Wuhan, 430079,
9 China

10 ² Central-South Architectural Design Institute Co.,Ltd. (CSADI), Wuhan, 430071,
11 China

12
13 Corresponding authors. E-mail addresses: fengwu@whu.edu.cn (Feng Wu);
14 327266781@qq.com (Jing Li)

15

Content

16

17

18 **List of texts:**

19

20 **Text S1.** Physicochemical characterization of material and methods

21

22 **List of Figure:**

23 **Figure S1.** FTIR spectra for (a) and (b) the raw and modified materials.

24 **Figure S2.** The energy-dispersive X-ray spectroscopy (EDS) element in the material.

25 **Figure S3.** (a) Adsorption and desorption curves of N₂, (b) distribution of pore size;

26 **Figure S4.** Comparison of arsenic removal between SBE/C 500 °C-3h, Fe₃O₄, and Fe-
27 SBE/C 500 °C;

28 **Figure S5.** The influences of a.c) adsorbent dosage, b.d) ratio of Fe⁺³/Fe⁺² on arsenic
29 adsorption;

30 **Figure S6.** Adsorption kinetic studies of As(III) and As(V);

31 **Figure S7.** Isotherm Langmuir, Freundlich, and Temkin model of As(III) and As(V)
32 adsorption;

33 **Figure S8.** Adsorption thermodynamic (Van't Hoff) plot;

34 **Figure S9.** Arrhenius plot of As(III) and As(V) adsorption

35 **Figure S10.** Reusability cycle of Fe-SBE/C for As(III) and As(V) adsorption.

36

37 **Text S1. Physicochemical characterization of material and methods**

38 1. Physicochemical characterization of material

39 This study examined the thermal degradation of the material by utilizing thermographic
40 analysis (TG) (STA PT1600 LINSEIS Germany) in an air environment. The heating
41 rate was set at $5\text{ }^{\circ}\text{C min}^{-1}$, starting from room temperature and reaching $1000\text{ }^{\circ}\text{C}$. The
42 value of pH_{PZC} was obtained using a Zeta potential analyzer (ZEN3690, Malvern, UK).
43 The pattern of X-ray diffraction (XRD) was acquired by employing $\text{Cu-K}\alpha$ radiation as
44 a source of an X-ray powder diffractometer (Mini Flex600, Rigaku, Japan) with an
45 operating configuration using a generator with 30 kV voltage and a tube current of 30
46 mA. The Fourier transform infrared spectroscopy (FTIR) was used to analyse the
47 functional groups of materials. Subsequently, surface area and pore size distribution
48 were quantified using a Belsorp-mini II, MicrotracBel, Japan, with calculations based
49 on the Brunauer-Emmett-Teller (BET) and Barrett-Joyner-Halenda (BJH) methods
50 within a P/P_0 range of 0.05 to 0.25. The surface and cross-sectional morphologies of
51 the adsorbent were scrutinized using scanning electron microscopy (SEM), specifically
52 the Sigma model from ZEISS, Germany. Lastly, the surface chemical states were
53 characterized using X-ray photoelectron spectroscopy (XPS) (Thermo Kalpha; Thermo
54 Escalab 250XI, USA).

55

56 **2. Kinetic Study**

57 For the kinetic study, the solution of As (III) and As(V) with a concentration of $50\text{ }\mu\text{g}$
58 L^{-1} was prepared in a 250 mL glass bottle reaction with the lid on. After adjusting the
59 pH's solution to neutral pH 7, the adsorbent 1 g L^{-1} was added and mixed in a water
60 bath rotary shaker with a controlled temperature of $25\pm 2\text{ }^{\circ}\text{C}$. The experiment was held
61 for 180 mins with samples taken at each time interval (0, 1, 5, 10, 20, 30, 60, 90, 120,

62 150, and 180 mins). The sample was taken and filtered through a 0.22 μ m PES filter and
63 poured into a plastic tube, then immediately added 0.25 mL HCl 1:1 to stop the reaction
64 and 0,25 mL thiourea-ascorbic acid solution. HG-AFS measured the concentration of
65 As (III) and As (V) with As(total) configuration.

66 These models were determined by utilizing the respective equations assigned to each
67 model.

68 The equation for pseudo-first-order is described as

$$69 \ln(q_e - q_t) = \ln(q_e) - k_1 t \quad (1)$$

70 The simplified version of the Elovich kinetic model equation, commonly employed to
71 describe chemisorption on adsorbents with significant heterogeneity, has been
72 presented by Chien and Clayton 1980 [1]. Equation (3) provides the expression for this
73 simplified model:

$$74 q_t = \frac{1}{\beta} \ln(\alpha\beta) + \ln t \frac{1}{\beta} \quad (3)$$

75 The parameters α and β correspond to the initial rate of adsorption (expressed in $\mu\text{g g}^{-1}$
76 min^{-1}) and desorption constant (expressed in $\text{g } \mu\text{g}^{-1}$), respectively.

77 The utilization of the intraparticle diffusion model allows for the investigation of
78 whether the adsorption process entails the movement of adsorbate molecules through
79 the pore of the adsorbent. Weber and Morris 1963 [2] established a framework that was
80 employed to assess this kinetic model. The equation representing the intraparticle
81 diffusion model is as follows:

$$82 q_t = K_{\text{diff}} t^{1/2} + C \quad (4)$$

83 The rate constant for intraparticle diffusion, denoted as K_{diff} , is expressed in $(\text{g } \mu\text{g}^{-1}$
84 $\text{min}^{1/2})^{-1}$ units. The coefficient C ($\mu\text{g g}^{-1}$) is also linked to the magnitude of the
85 boundary layer's thickness.

86

87 3. Isotherm study

88 In an isotherm study, 1 g L⁻¹ of adsorbent Fe-SBE/C was added to As(III) and As(V)
89 solution in 250 mL glass bottle with a vary concentration range from 10 - 250 µg L⁻¹
90 and mixed in a water bath rotary shaker with controlled temperature at 25±2 °C. HG-
91 AFS measured the concentration of As (III) and As(V) with As Total configuration. The
92 reactions were conducted with duplicate, and the initial pH was 7 for As(III) and pH 3
93 for As(V).

94 The adsorption isotherm concept describes how adsorbed molecules are distributed
95 between the liquid and should phase at equilibrium. The present study evaluated the
96 equilibrium adsorption data for As(III) and As(V) on Fe-SBE/C using three different
97 isotherm models. First, the isotherm Langmuir model explains the quantitative
98 information of monolayer molecules on the adsorbent's surface, which is affected by
99 the concentration of the adsorbed substance in the liquid phase. Mathematically, the
100 Langmuir model isotherm can be expressed by the equation [3]:

$$101 \quad q_e = q_{\max} \cdot C_e K_L / (1 + C_e K_L) \quad (5)$$

102 In the context of this study, the variable q_e (µg g⁻¹) represents the quantity of arsenic
103 that has been adsorbed at the point of equilibrium. q_{\max} (µg g⁻¹) denotes the maximum
104 capacity of the adsorbent material to uptake arsenic. K_L (L µg g⁻¹) serves as the
105 equilibrium constant, crucial in determining the overall adsorption process. Lastly, C_e
106 (µg L⁻¹) represents the equilibrium concentration of arsenic.

107 Second, Freundlich isotherm, a renowned empirical equation, describes the adsorption
108 phenomenon occurring on a surface that displays heterogeneity in its heat of adsorption
109 distribution. This surface, which accommodates the adsorbed molecules interacting
110 with each other, showcases diverse energetic characteristics. The Freundlich isotherm
111 can be represented as follows [4]:

112 $q_e = K_F C_e^{1/n}$ 6)

113 The parameter q_e ($\mu\text{g g}^{-1}$) is the significant amount of adsorbed mass per unit of the
114 adsorbent when equilibrium is reached. C_e ($\mu\text{g L}^{-1}$) is denoted as the equilibrium
115 concentration of arsenic. K_F and $1/n$ are also essential as they denote the adsorption
116 capacity and intensity, respectively.

117 Third, the Temkin isotherm model assumes that the decrease in the heat of adsorption
118 for each molecule within the adsorbent layer follows a linear trend as the coverage
119 increases. The phenomenon arises from the interactions between the sorbate and sorbent.
120 The following equation represents this Temkin isotherm model [5]:

121 $q_e = B \ln A.C_e$ 7)

122 The equation $B = RT/bt$ represents the relationship between the heat of adsorption
123 (J mol^{-1}) and the temkin isotherm constant (L g^{-1}). Here, R represents the gas constant
124 ($8.314 \text{ J mol}^{-1} \text{ K}$), and T denotes the absolute temperature (K).

125 **4. Thermodynamics**

126 The investigation examined the adsorption kinetic across varying temperatures: 25°C ,
127 35°C , and 40°C . The findings of this study align with the commonly observed
128 phenomenon that higher temperatures tend to enhance the adsorption capacity. In order
129 to ascertain the parameters of thermodynamics, including the standard Gibbs free
130 energy (ΔG°), change of enthalpy (ΔH°), and change in entropy (ΔS°), the established
131 equation was utilized.

132 $\Delta G^\circ = -RT \ln K_L$ (8)

133 According to Maiti et al. [6,7], the equilibrium constant, denoted as K_L , can be
134 expressed as $K_L = q_e/C_e$. In this equation, q_e represents the equilibrium concentration
135 of arsenic in the solution, while C_e refers to the concentration reduced by the adsorbent
136 due to adsorption at equilibrium.

137 The equation below encompasses the relationship between the change in enthalpy
138 (ΔH°), and change in entropy (ΔS°), and the Gibb's free energy:

$$139 \ln K_L = \Delta S^\circ/R - \Delta H^\circ/RT \quad (9)$$

140 The values for both changes were derived from the intercept and slope of the $\ln K_L$ vs
141 $1/T$ curves (Van't Hoff plot).

142 The activation energy (E_a , KJ mol^{-1}) has been calculated using Arrhenius equation [8,9]:

$$143 \ln k_{app} = \ln A - E_a/RT \quad (10)$$

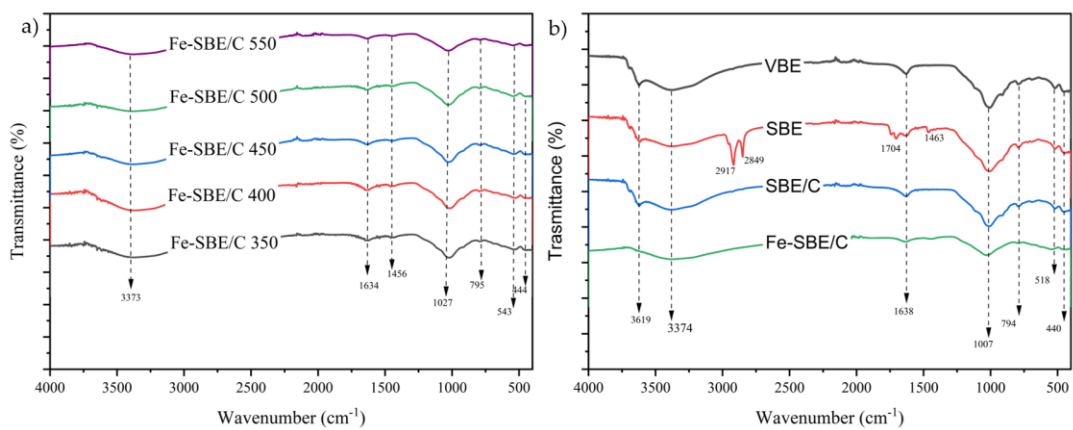
144 k_{app} is the apparent pseudo-first order rate constant, A is the Arrhenius constant (J mol^{-1}
145 K^{-1}). In equations (9) and (10), T denotes the temperature in Kelvin and R denotes the
146 universal gas constant ($\text{J mol}^{-1} \text{K}$).

147 **5. Regeneration and reusability study**

148 Four consecutive cycles were conducted to evaluate the regeneration and reusability of
149 the composite through adsorption-desorption experiments. The adsorbent's surface
150 becomes negatively charged when exposed to an alkaline solution. As a result, As(III)
151 primarily exists as a divalent anion. This causes the adsorbed arsenic to be released
152 from the surface of the materials [10]

153 The desorption of the composite loaded with As(III) is performed with a 0.1 mol L^{-1}
154 NaOH as the agent for desorption. An adsorbent with a concentration of 1 g L^{-1} was
155 individually mixed with NaOH solution. The mixture was then placed in a thermostatic
156 shaker and agitated for 180 minutes at 250 rpm. Upon concluding the experiment, the
157 solution underwent filtration and was subsequently stored for subsequent analysis. The
158 solid was rinsed in three cycles using Ultrapure water and then utilized for another
159 adsorption process. The adsorption process was repeated three times consecutively.

160 **Supplementary of Figure**

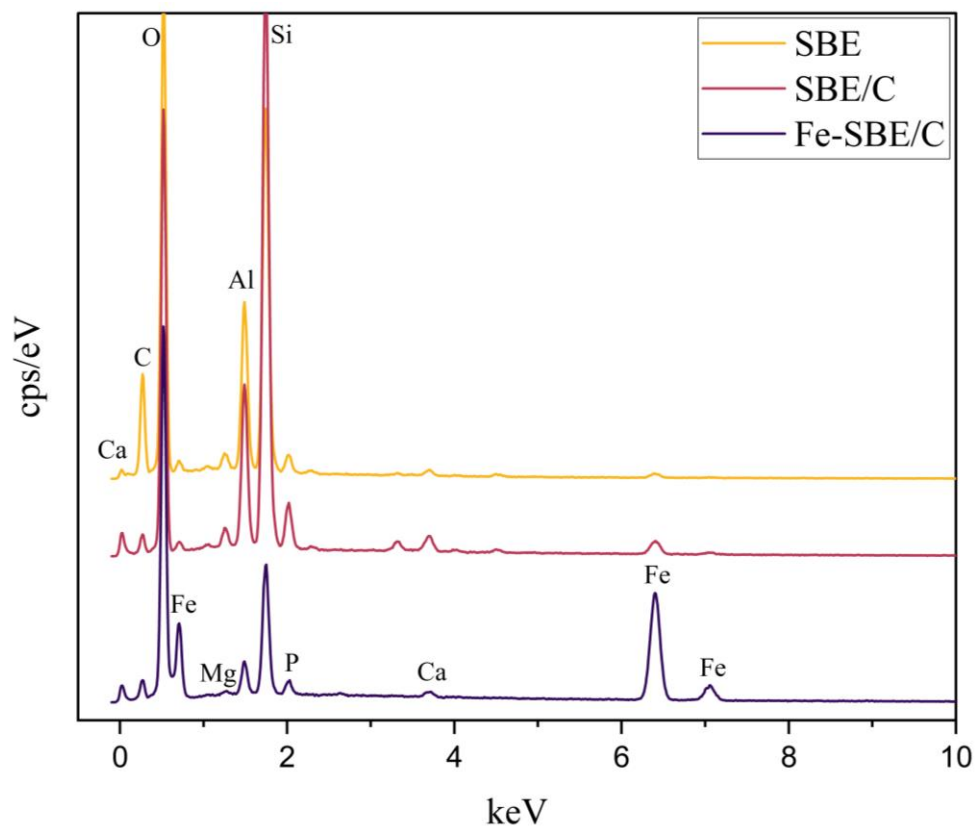


161

162 **Figure S1.** FTIR spectra for (a) the modified materials at different calcination

163 temperatures and (b) the materials VBE and SBE, SBE/C, and Fe-SBE/C

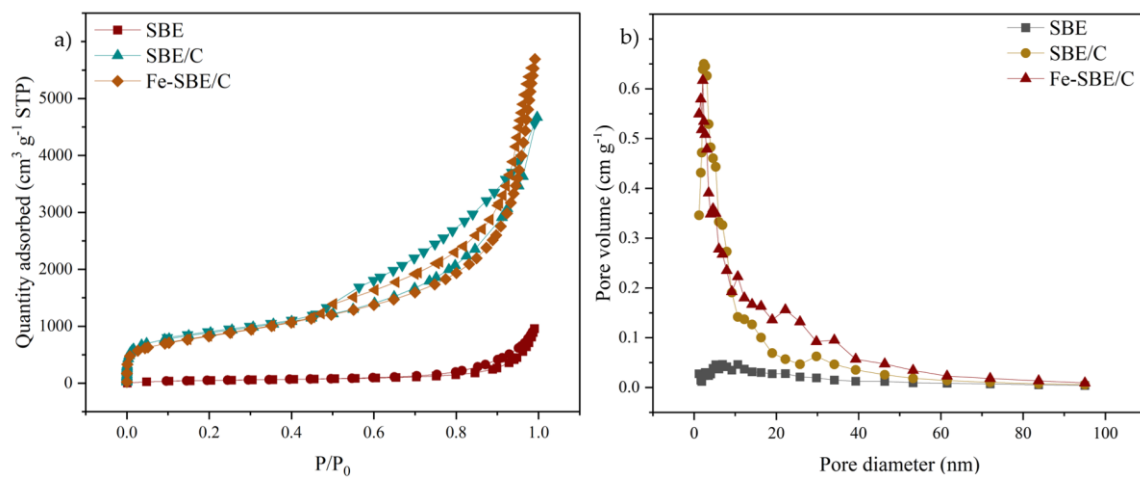
164



165

166 **Figure S2.** The energy-dispersive X-ray spectroscopy (EDS) element in the material.

167

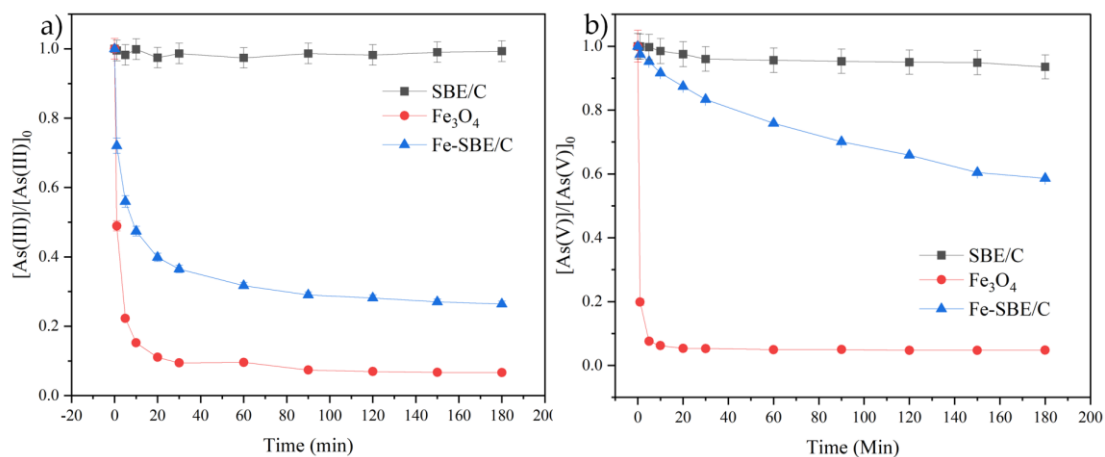


168

169 **Figure S3.** (a) Adsorption and desorption curves of N₂, (b) distribution of pore size.

170

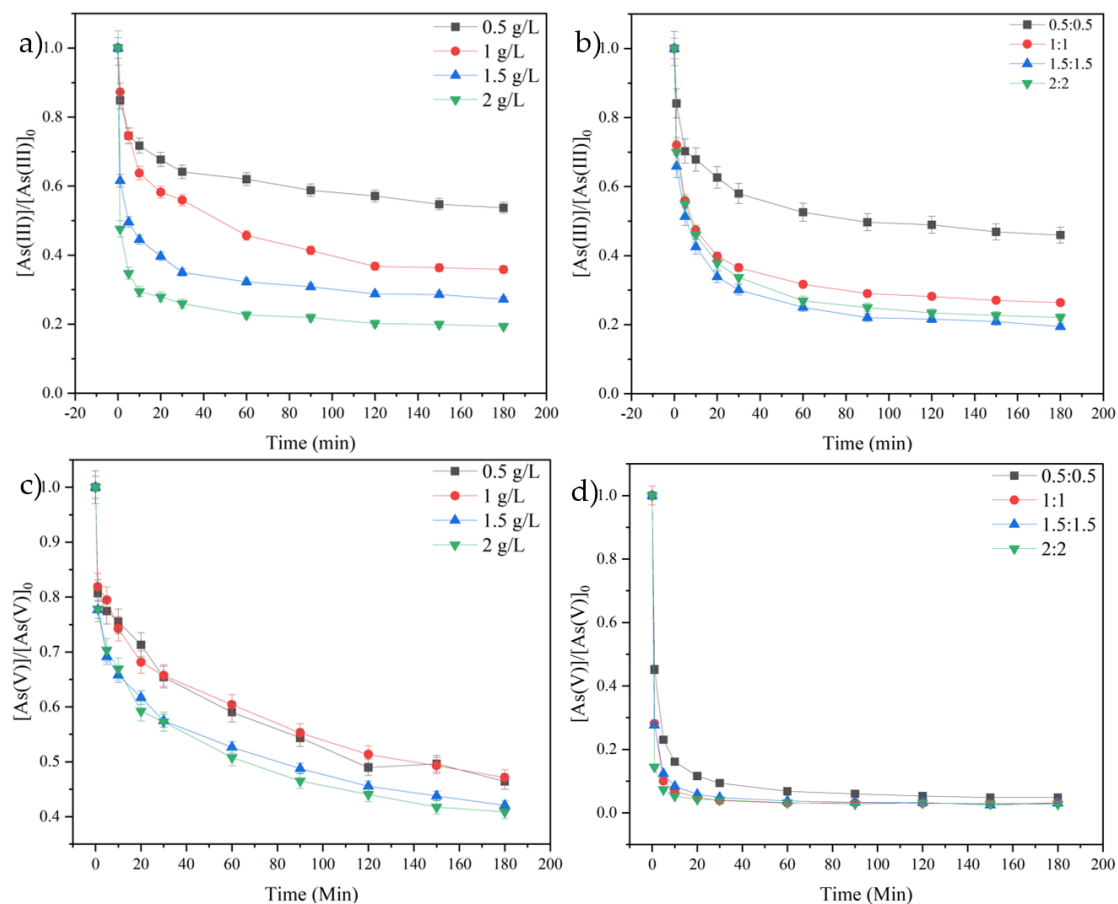
171



172

173 **Figure S4.** Comparison of (a) As(III) and (b) As(V) removal between SBE/C 500 °C-
 174 3h, Fe₃O₄, and Fe-SBE/C 500 °C. Experimental conditions: Adsorbent dosage = 1 g L⁻¹;
 175 V = 250 mL; initial concentration of arsenic = 50 μg L⁻¹; pH = 7; T = 25°C; S = 250
 176 rpm; t = 3 h.

177



178

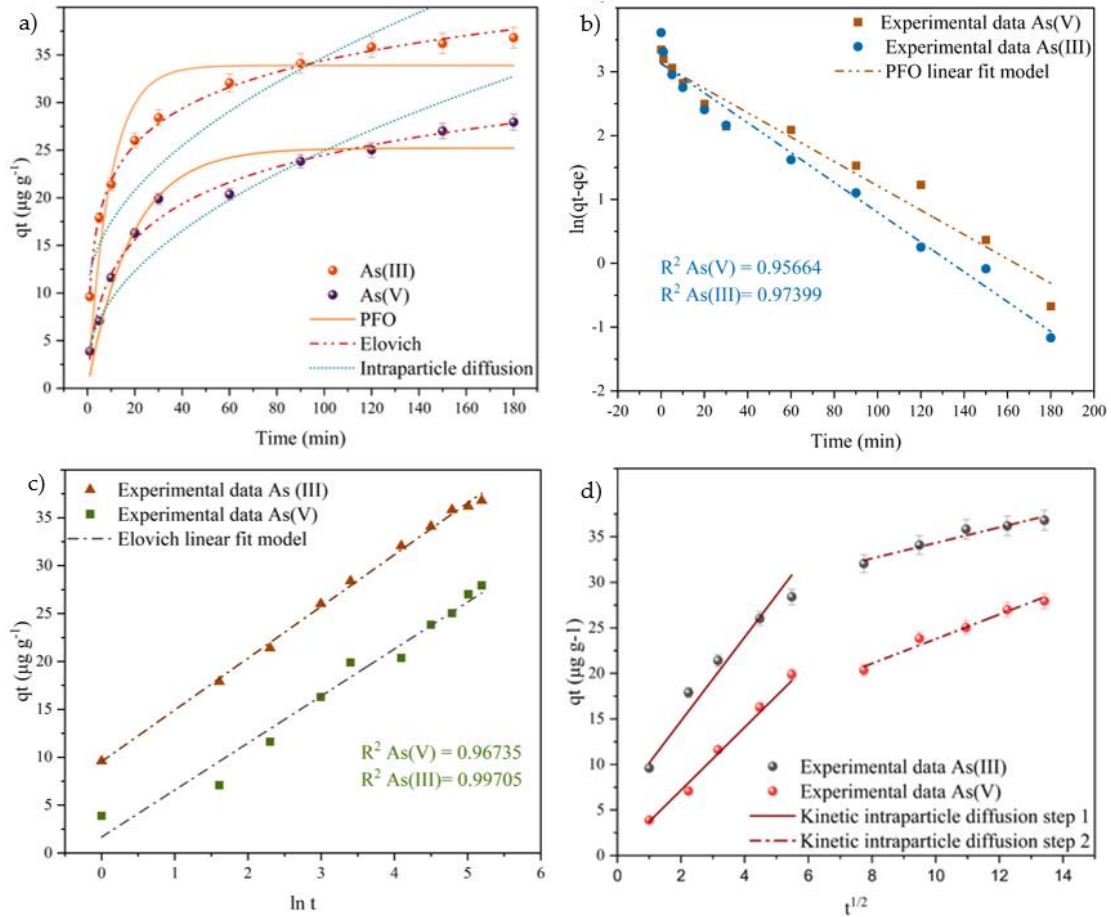
179 **Figure S5.** The influences of adsorbent dosage (**a** and **c**), the ratio of Fe(III)/Fe(II) (**b**

180 and **d**) on As(III)/As(V) adsorption, respectively. Experimental conditions: (iron ratio;

181 Adsorbent dosage = 1 g L⁻¹); V = 250 mL; Initial concentration of arsenic = 50 μg L⁻¹;

182 (adsorbent dosage: pH = 7 (As(III)) and pH 3 (As(V))) T = 25°C; S = 250 rpm; t = 3 h.

183



184

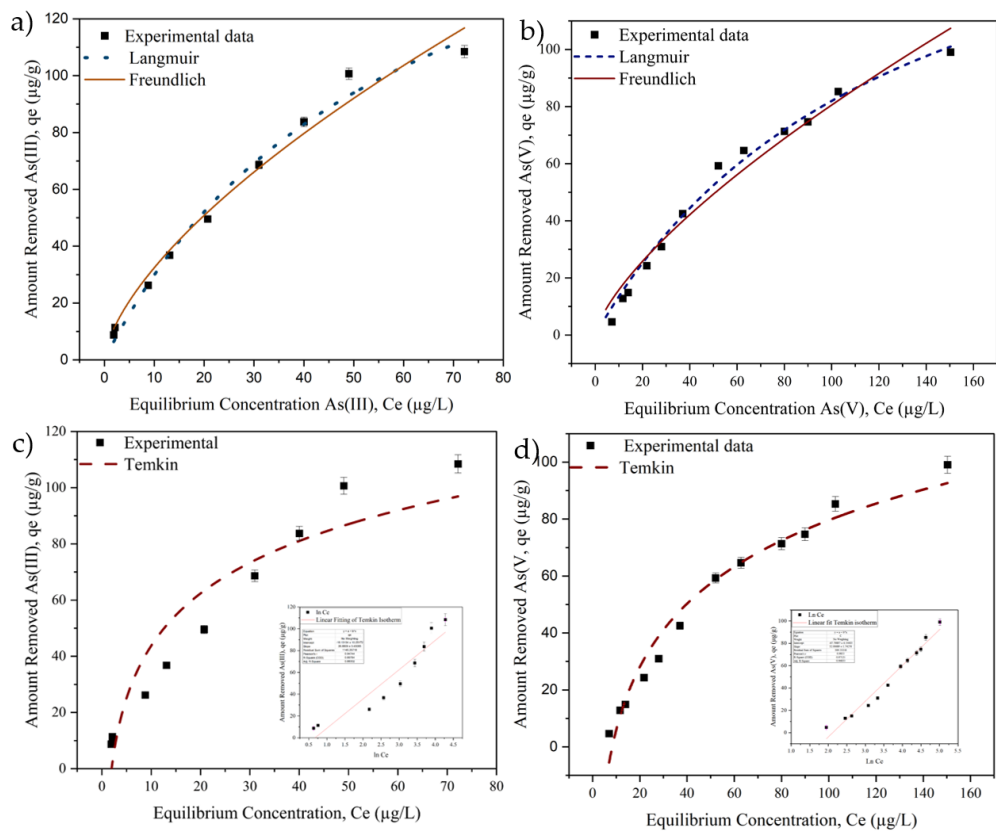
185 **Figure S6.** Adsorption kinetic studies of As(III) and As(V), (a) Kinetic models, (b)

186 Pseudo-first-order linear fit model, (c) Elovich linear fit model, (d) Intraparticle

187 diffusion model. Experimental conditions; Adsorbent dosage = 1 g L^{-1} ; $V = 250\text{ mL}$;

188 Initial concentration of arsenic $50\text{ }\mu\text{g L}^{-1}$; $\text{pH} = 7$; $T = 25\text{ }^\circ\text{C}$; $S = 250\text{ rpm}$; $t = 3\text{ h}$.

189



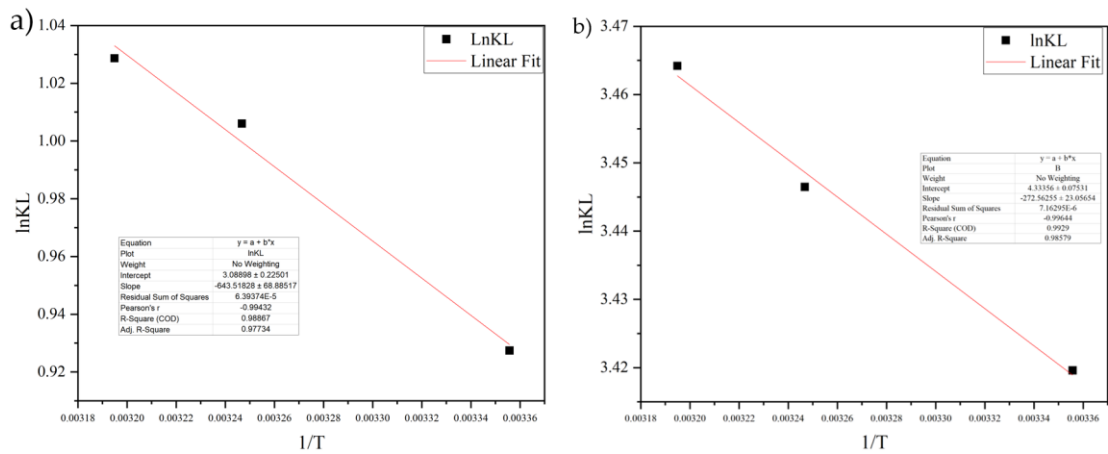
190

191 **Figure S7.** Isotherm Langmuir, Freundlich, and Temkin model of As(III) (a and c) and

192 As(V) (b and d) adsorption. Experimental conditions; Adsorbent dosage= 1g L⁻¹, V =

193 250 mL; T= 25 °C; t= 3 h; S= 250 rpm; pH= 7 (As(III)), pH=3 (As(V)).

194



195

196 **Figure S8.** Adsorption thermodynamic (Van't Hoff) plots for adsorption of As(III) (a)

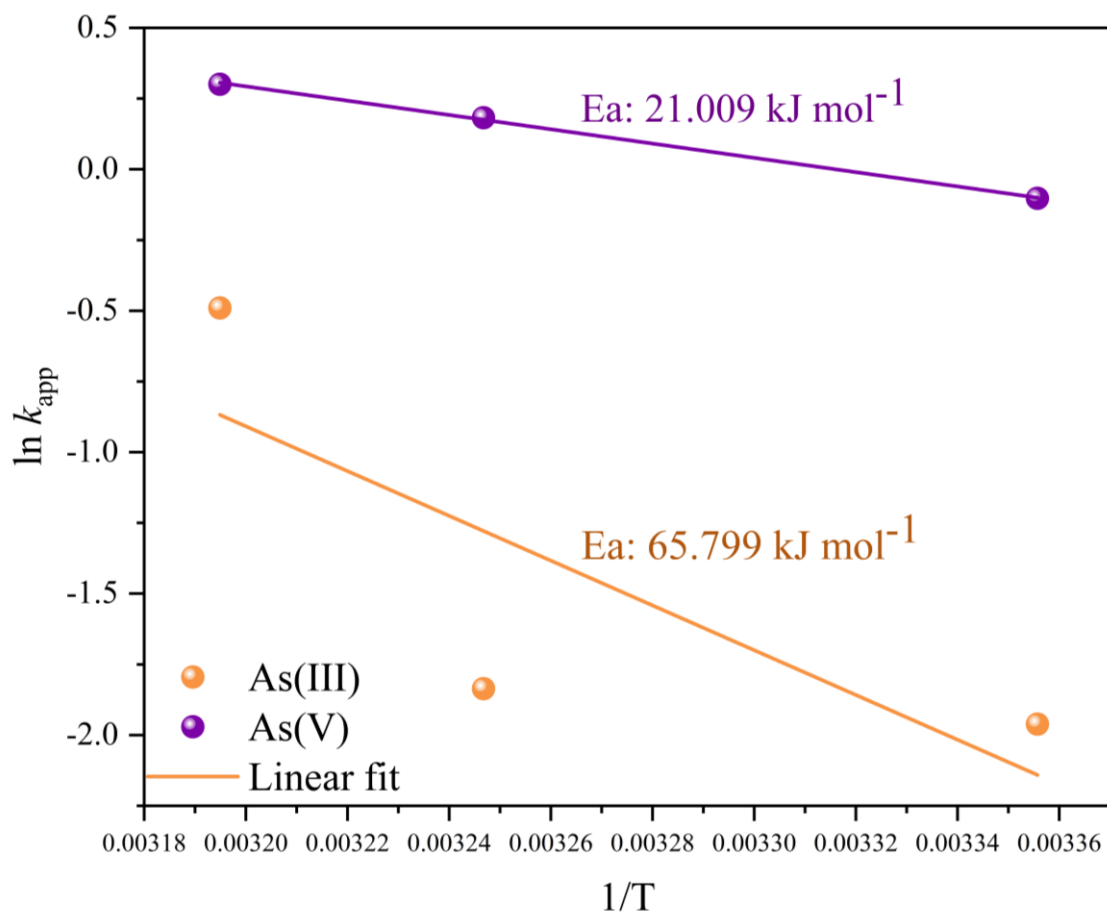
197 and As(V) (b). Experimental condition; Adsorbent dosage = 1 g L⁻¹; V= 250 mL; Initial

198 concentration of arsenic = 50 µg L⁻¹; T= 25 °C, 35 °C, and 40 °C; t = 3 h; S= 250 rpm,

199 pH = 6 for As(III) and pH = 3 for As(V).

200

201



202

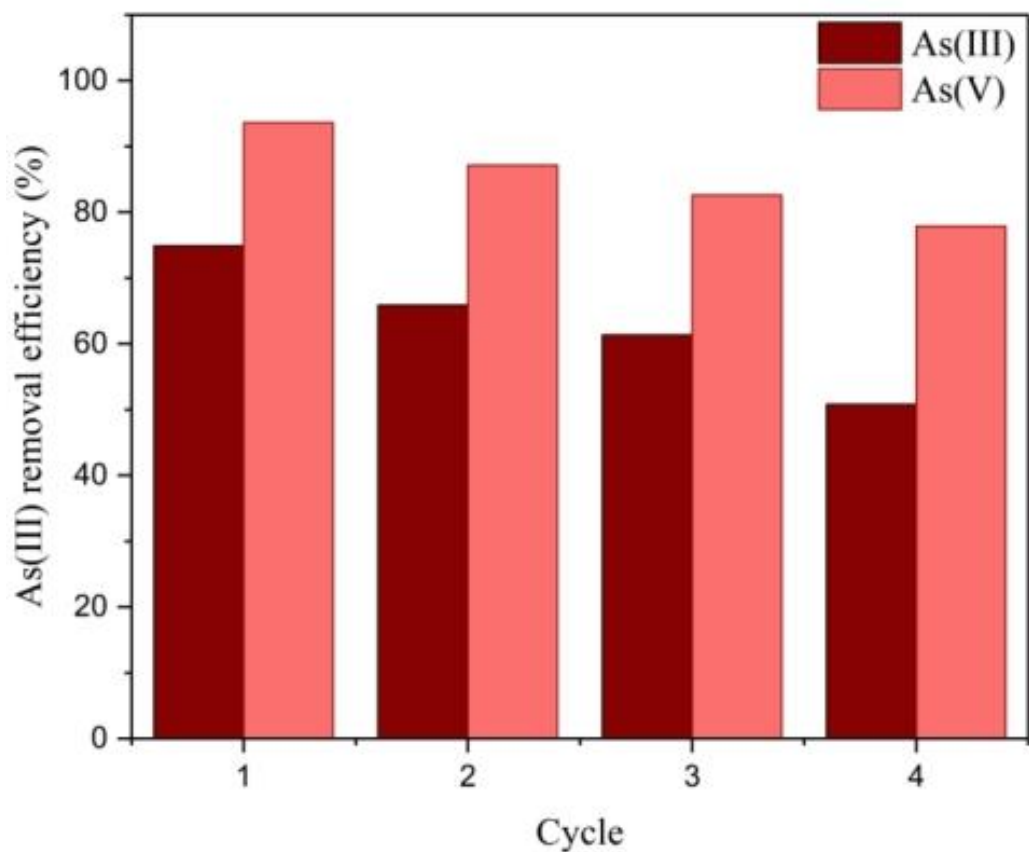
203 **Figure S9:** Arrhenius plot of As(III) and As(V) adsorption. Experimental condition;

204 Adsorbent dosage = 1 g L⁻¹; V= 250 mL; Initial concentration of arsenic = 50 µg L⁻¹;

205 T= 25 °C, 35 °C, and 40 °C; t = 3 h; S= 250 rpm, pH = 6 for As(III) and pH = 3 for

206 As(V).

207



208

209 **Figure S10.** Reusability cycle of Fe-SBE/C for As(III) and As(V) adsorption.

210 Experimental conditions; Adsorbent dosage= 1 g L⁻¹, V = 250 mL; Initial concentration

211 of arsenic = 50 µg L⁻¹; T= 298K; t= 3 h; S= 250 rpm; pH= 7 for As(III) and pH=3 for

212 As(V).

213

214 **References**

- 215 1. Chien, S.H.; Clayton, W.R. Application of Elovich Equation to the Kinetics of
216 Phosphate Release and Sorption in Soils. *Soil Sci. Soc. Am. J.* **1980**, *44*, 265–268,
217 doi:10.2136/sssaj1980.03615995004400020013x.
- 218 2. Weber, W.J.; Morris, J.C. Kinetics of Adsorption on Carbon from Solution. *J.*
219 *Sanit. Eng. Div.* **1963**, *89*, 31–59, doi:10.1061/JSEDAI.0000430.
- 220 3. Langmuir, I. The Adsorption of Gasses on Plane Surface, Mica and Platinum. *J.*
221 *Am. Chem. Soc.* **1918**, *40*, 1361–1403, doi:10.1021/ja02242a004.
- 222 4. Freundlich, H. Kapillarchemie: Eine Darstellung Der Chemie Der Kolloide Und
223 Verwandter Gebiete. *Akad. Verlagsgesellschaft*, **1922**.
- 224 5. Temkin, M.; Pyzhev, V. Kinetics of Ammonia Synthesis on Promoted Iron
225 Catalysts. *Acta Physicochim. URSS* **1940**, *12*, 217-222.
- 226 6. Maiti, A.; DasGupta, S.; Basu, J.K.; De, S. Adsorption of Arsenite Using Natural
227 Laterite as Adsorbent. *Sep. Purif. Technol.* **2007**, *55*, 350–359,
228 doi:10.1016/j.seppur.2007.01.003.
- 229 7. Asere, T.G.; Stevens, C. V.; Du Laing, G. Use of (Modified) Natural Adsorbents
230 for Arsenic Remediation: A Review. *Sci. Total Environ.* **2019**, *676*, 706–720,
231 doi:10.1016/j.scitotenv.2019.04.237.
- 232 8. Benjamin, M.M.; Leckie, J.O. Multiple-Site Adsorption of Cd, Cu, Zn, and Pb
233 on Amorphous Iron Oxyhydroxide. *J. Colloid Interface Sci.* **1981**, *79*, 209–221,
234 doi:10.1016/0021-9797(81)90063-1.
- 235 9. Ebelegi, A.N.; Ayawei, N.; Wankasi, D. Interpretation of Adsorption
236 Thermodynamics and Kinetics. *Open J. Phys. Chem.* **2020**, *10*, 166–182,
237 doi:10.4236/ojpc.2020.103010.
- 238 10. Ranjan, S.; Yadav, B.K.; Joshi, H. Removal of Arsenic (III and V) from Aqueous
239 Solution Using Stable Maghemite (γ -Fe₂O₃) Loaded Pumice Composite. *Int. J.*
240 *Environ. Sci. Technol.* **2022**, *19*, 4737–4748, doi:10.1007/s13762-021-03326-x.
- 241